Phonon-polariton damping by low-frequency excitations in lithium tantalate investigated by spontaneous and stimulated Raman scattering

2002 J. Phys.: Condens. Matter 14 9013

(http://iopscience.iop.org/0953-8984/14/39/311)

INSTITUTE OF PHYSICS PUBLISHING JOURNAL OF PHYSICS: CONDENSED MATTER

J. Phys.: Condens. Matter **14** (2002) 9013–9028 PII: S0953-8984(02)37637-9

Phonon-polariton damping by low-frequency excitations in lithium tantalate investigated by spontaneous and stimulated Raman scattering

B Bittner, M Scherm, T Schoedl, T Tyroller, U T Schwarz[1] and Max Maier

Naturwissenschaftliche Fakultät II–Physik, Universität Regensburg, D-93040 Regensburg, Germany

E-mail: uli.schwarz@physik.uni-regensburg.de

Received 31 May 2002
Published 19 September 2002
Online at stacks.iop.org/JPhysCM/14/9013

Abstract

We investigated the damping of phonon polaritons in congruent lithium tantalate ($LiTaO_3$) single crystals by measuring spontaneous Raman spectra of the low-frequency wing of the A_1 phonon line, the dependence of the linewidth of the stimulated Raman scattering gain curves on polariton frequency and the spatial damping of propagating phonon-polariton pulses by nonlocal time-delayed coherent anti-Stokes Raman scattering. The damping and the dispersion curve of the lowest-frequency A_1 phonon polaritons were determined from 10 to 200 cm^{-1} at room temperature and at 77 K. The observed frequency dependence of the damping is discussed in the context of low-frequency excitations and a Debye relaxational mode.

1. Introduction

The ferroelectric crystal lithium tantalate ($LiTaO_3$) is a material of widespread use predominately for nonlinear optical and electro-optical applications. $LiTaO_3$ can be grown with high optical quality and a variety of dopants to control the linear and nonlinear optical properties [1, 2]. The electro-optic and ferro-electric properties are dominated by low-frequency phonon modes. A phonon mode of A_1 symmetry at about 200 cm^{-1} is related to the paraelectric–ferroelectric phase transition which occurs at a relatively high temperature of 665 °C [1]. The far-infrared (FIR) absorption and nonlinear optical response are dominated by additional low-frequency modes below 200 cm^{-1} which are not extended phonon modes associated with the C_{3v} crystal symmetry of $LiTaO_3$ [3–5]. In ferroelectric $LiNbO_3$ a low-frequency mode at approximately 110 cm^{-1} could be associated with a defect mode. Its

[1] www.physik.uni-regensburg.de/forschung/maier/index.html

strength and shape varies with doping or the concentration of intrinsic defects in the individual crystal [6]. Though other methods were employed to clarify the origin of these modes (for an overview see [7]), they are most prominent in Raman scattering experiments performed on phonon polaritons [4, 8, 9].

For the investigation of phonon polaritons five different Raman schemes have been used, which differ in excitation, detection and timescale: spontaneous Raman scattering, stimulated Raman scattering (SRS), nonlocal time-delayed coherent anti-Stokes Raman scattering (CARS), impulsive SRS and real-time imaging of polariton wavepackets. Spontaneous Raman scattering and the SRS amplifier experiment [6, 10] with nanosecond pulses are stationary in space and time on the scale of phonon-polariton damping. Nonlocal time-delayed CARS with picosecond pulses measures the spatial damping in a direct way, observing the phonon-polariton decay while the polariton pulse propagates through the crystal [11, 12]. Impulsive SRS with femtosecond pulses, which are short compared to a single phonon-polariton cycle, measure the phonon-polariton amplitude [4, 5, 13]. Here low-frequency modes show up as beat frequencies [9]. Real time imaging of polariton wavepackets combines the impulsive excitation with femtosecond pulses and a nonlocal detection scheme [14, 15].

The purpose of this article is twofold. First we provide a complete set of experimental data for damping and dispersion of the A_1 phonon polariton in lithium tantalate from 10 to 200 cm^{-1} at temperatures of 77 and 295 K. For $T = 77$ K no SRS experiments for $LiTaO_3$ have been published. At $T = 300$ K damping and dispersion measurements exist from 30 up to 160 cm^{-1} [5], which we will compare with our results. We carried out three different types of Raman experiment. From the measurement of spontaneous Raman scattering at a scattering angle of 90° we determine the resonance frequencies and damping constants of the low-frequency modes in the whole frequency range from 10 to 200 cm^{-1}. The measurement of the gain curves for near forward SRS provides the damping and the dispersion relation of the polaritons between 70 and 200 cm^{-1}. In the polariton frequency range between 10 and 70 cm^{-1} the corresponding quantities are obtained by investigating the propagation dynamics of free polariton pulses by nonlocal time-delayed coherent anti-Stokes Raman scattering. From this first measurement of the complete phonon-polariton branch at 77 K we provide frequency, linewidth and coupling strength for ten low-frequency modes below 200 cm^{-1}. The precision of the dispersion curve measured by stimulated Raman gain measurements surpasses those measured by other Raman methods by at least one order of magnitude. It allows us to study the influence of the low-frequency modes on the phonon-polariton dispersion curve in detail.

Second we want to compare the different Raman experiments to test whether they can be described in the framework of an existing theory with one set of parameters for the dielectric function. For this comparison spontaneous and stimulated Raman experiments were performed on one individual $LiTaO_3$ crystal to eliminate variations due to different composition and doping. We use the specific ansatz of the linear response function theory adapted by Barker and Loudon for phonon-polariton Raman scattering [16]. The gain ansatz [17, 18] usually used to describe phonon-polariton Raman scattering can be derived from linear response theory. Using the dielectric function $\varepsilon(\omega)$ to describe the material properties, we will demonstrate that all experimental data can be described by this general linear response ansatz, with one exception: at $T = 77$ K two different sets of parameters for the coupling strength of the low-frequency modes to the polariton are needed to describe spontaneous and stimulated Raman scattering experiments, respectively. Several explanations of this observation are discussed; one suggestion is that these coupling constants and the resulting dielectric function $\varepsilon(\omega, k)$ depend both on frequency and wavevector of the excited polariton.

2. Theory

2.1. Single-phonon model

In this section we present a unified description of our experimental investigations based on the dielectric function $\varepsilon(\omega)$ of the material. To derive the expressions for spontaneous and stimulated Raman scattering experiments we start with a single polar phonon mode with frequency ω_0, damping constant Γ_0 and oscillator strength S_0. The dielectric function $\varepsilon = \varepsilon' + i\varepsilon''$ is then given by

$$\varepsilon(\omega) = \varepsilon_\infty + \frac{S_0\omega_0^2}{\omega_0^2 - \omega^2 - i\omega\Gamma_0}. \tag{1}$$

Higher-frequency phonon modes are taken into account using an effective dielectric constant ε_∞. The oscillator strength S_0 is given by

$$S_0 = \frac{NZ_0^{*2}}{\varepsilon_0 m_0 \omega_0^2}, \tag{2}$$

where N is the number density of primitive cells, and Z_0^* and m_0 are the effective charge and reduced mass of the ions, respectively.

In the time-delayed CARS experiment the absorption coefficient $\alpha(\omega)$ and group velocity $v_{gr}(\omega)$ for freely propagating polaritons are measured, which can be calculated directly from ε [11, 12].

The differential scattering cross section $d^2\sigma/(d\Omega\, d\omega_S)$ for spontaneous Raman scattering and the gain factor g_S for SRS are proportional to each other and can be derived using a linear response function theory [16]. Frequency $\omega = \omega_L - \omega_S$ and wavevector $\boldsymbol{k} = \boldsymbol{k}_L - \boldsymbol{k}_S$ of the excited polariton are forced by the driving laser pump and Stokes fields, which are denoted by the indices L and S, respectively. It is important to note that wavevector $\boldsymbol{k}$ and frequency ω of the excited polariton are therefore not necessarily related via the polariton dispersion relation. The gain factor $g_S(\omega, k)$ has to be written as a function of the frequency ω and wavevector k of the driven polariton and is given by [6, 17, 18]

$$g_S(\omega, k) = \frac{2\omega_S}{\varepsilon_0 c^2 n'_S n'_L} \mathrm{Im}\left\{ \frac{[d'_Q(\varepsilon - \varepsilon_\infty) + 2d'_{33}]^2}{\frac{c^2k^2}{\omega^2} - \varepsilon} + d'^2_Q(\varepsilon - \varepsilon_\infty) \right\}. \tag{3}$$

Here c is the light velocity in vacuum, ε_0 the dielectric constant of the vacuum and n'_S and n'_L are the real parts of the refractive indices for the Stokes and pump light, respectively. The nonlinear coefficients d'_{33} and d'_Q take into account the electronic and vibrational contributions to the amplification process. The coefficient d'_Q is defined in the following way:

$$d'_Q = d_Q/Z_0^* \tag{4}$$

where d_Q is proportional to the change $d\alpha/dq$ of the polarizability α with vibrational coordinate q and Z_0^* is the effective charge of the ions. It can be shown that the first term in the curly brackets of equation (3) is dominant for near forward scattering (small scattering angles and k vectors), while the second term is important for large scattering angles (e.g. 90°) and large k vectors.

Figure 1 shows the gain factor g_S as a function of polariton wavenumber $\bar{\nu} = \omega/(2\pi c)$ and wavevector k as a shaded surface in a three-dimensional plot. The minimum at about $\bar{\nu}_j = 90\ \mathrm{cm}^{-1}$ in figure 1 is due to the inclusion of a low-frequency mode, which will be discussed in the next section. The solid curve is the perpendicular projection of the peak values of $g_S(\bar{\nu}, k)$ into the $\bar{\nu}$–k plane; it corresponds to the polariton dispersion curve [4, 6, 16]. We used this definition of the polariton dispersion curve which is given by Barker and Loudon [16],

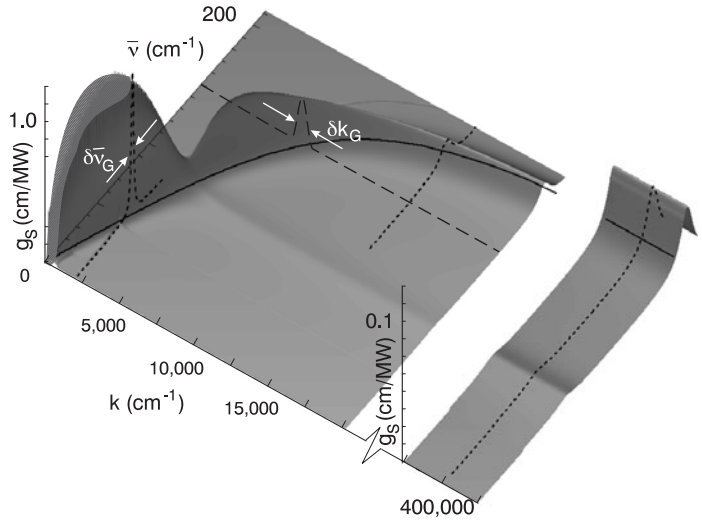

Figure 1. Three-dimensional plot of the Raman gain factor $g_S(\bar{\nu}, k)$ as a function of the polariton wavenumber $\bar{\nu}$ and wavevector k. The shaded surface is calculated using equations (3) and (8) with one single low-frequency excitation at $\bar{\nu}_j = 90$ cm^{-1}. The dotted and dashed curves are the intersecting curves of the $g_S(\bar{\nu}, k)$-surface along constant k and along constant $\bar{\nu}$, respectively (g_S-scale is changed at $k \approx 4 \times 10^5$ cm^{-1}). The solid curve is the polariton dispersion curve (for details see text).

and not the usual definition, involving the real parts of the polariton frequency and wavevector using equation (1).

The measurements of the Raman gain factor were carried out in two ways, for nearly constant polariton wavevector k or constant wavenumber $\bar{\nu}$, i.e., they correspond to the intersecting curves of the planes of constant k (dotted) or constant $\bar{\nu}$ (dashed) with the shaded $g_S(\bar{\nu}, k)$ surface (figure 1). The widths (full width at half maximum (FWHM)) $\delta\bar{\nu}_G$ and δk_G of these gain curves contain the information on the temporal and spatial damping of the polaritons, respectively.

Wiederrecht *et al* [5] have introduced a temporal polariton damping constant γ_P which is calculated as the imaginary part of the complex polariton frequency ω by solving the dispersion relation for real wavevectors k. The Raman linewidth $\delta\bar{\nu}_G$ is related to γ_P by $\delta\bar{\nu}_G = 2\gamma_P$. The phase relaxation time T_2 of the polaritons, which has been used in [11], is given by $T_2 = (\pi c \delta\bar{\nu}_G)^{-1}$.

The width δk_G of the gain curve for constant polariton *wavenumber* $\bar{\nu}$ (dashed line in figure 1) contains information on the spatial damping of the polaritons. It has been shown in [16] that far from the resonance frequency ω_0 of the phonon, for $\varepsilon'' \ll \varepsilon'$, the width δk_G is approximately equal to the absorption coefficient α of freely propagating polaritons.

Temporal and spatial damping of polaritons are related via the group velocity v_{gr} in the following way:

$$\delta\bar{\nu}_G \approx \delta k_G v_{gr}/(2\pi c) \approx \alpha v_{gr}/(2\pi c). \tag{5}$$

This expresses the geometrical relation between $\delta\bar{\nu}_G$ and δk_G as cuts in the $\boldsymbol{k}$ and $\bar{\nu}$ directions, respectively, through the polariton ridge $g_S(\bar{\nu}, k)$ in figure 1 using the slope $\partial\bar{\nu}/\partial k = v_{gr}/(2\pi c)$ of the dispersion curve. This is valid as long as the curvature of the ridge is small, but cannot be used close to where the polariton dispersion is split by a coupling to a low-frequency mode [9].

Spontaneous Raman spectra measured at a scattering angle of 90° at constant wavevector k give information on the polaritons with very large wavevectors k which are practically phonons (see dotted curve at $k \approx 4 \times 10^5$ cm^{-1} in figure 1). The spontaneous Raman scattering cross section is obtained from the gain factor g_S by multiplication with the phonon occupation number $n(\omega, T) = [\exp(\hbar\omega/k_B T) - 1]^{-1}$. In the limit of large polariton wavevectors k the first term in the curly brackets of equation (3) is negligible, reducing the 90° spontaneous Raman scattering cross section to the familiar simple expression [16]

$$\frac{\mathrm{d}^2\sigma}{\mathrm{d}\Omega\,\mathrm{d}\omega_S} \propto [n(\omega, T) + 1] d_Q'^2 \,\mathrm{Im}\{\varepsilon(\omega)\}, \tag{6}$$

which represents for $\omega_0 - \omega \ll \omega_0$ in a good approximation a Lorentzian Raman line with a width Γ_0 (FWHM) using $\varepsilon(\omega)$ from equation (1). The intensity of the spontaneous 90° Raman line is proportional to $d_Q'^2 S_0$ (see equations (1) and (6)). Using the definitions of S_0 (equation (2)) and d_Q' (equation (4)) it can be shown that this product is proportional to $(\mathrm{d}\alpha/\mathrm{d}q)^2$, the change of the polarizability with vibrational coordinate, but is independent of the effective charge Z_0^* of the ions, as expected for 90° scattering.

The above discussion shows that equations (3) and (6) contain in principle all information needed for the interpretation of our results obtained by the measurement of the gain factor for SRS, the spontaneous Raman spectra and the free propagation of the polaritons in the crystal. The material properties are described by the dielectric function ε and the nonlinear coefficients d_{33}' and d_Q'. However, in practice the advantages and disadvantages of the different experimental methods depend on the frequencies of the investigated polaritons.

2.2. *Extensions of the model*

The single-phonon model presented in the preceding section leads to a spontaneous Raman line shape of the phonon mode which is described in a good approximation by a Lorentzian function (equations (1) and (6)). Since the low-frequency wing of the 203 cm^{-1} Raman line in $LiTaO_3$ is better represented by a Gaussian curve at temperatures below 100 K (see section 3.1), we tentatively suggest that the line is inhomogeneously broadened. The Gaussian distribution with width $\delta\omega_0$ of Lorentzian lines with resonance frequencies ω_0' results in a Voigt profile for the dielectric function:

$$\varepsilon(\omega) = \varepsilon_\infty + \frac{S_0\omega_0^2}{\sqrt{\pi}\delta\omega_0} \int_{-\infty}^{\infty} \frac{\exp\left[-\left(\frac{\omega_0'-\omega}{\delta\omega_0}\right)^2\right]}{\omega_0'^2 - \omega^2 - \mathrm{i}\omega\Gamma_0}\,\mathrm{d}\omega_0'. \tag{7}$$

Here it is assumed that all oscillators have the same damping constant Γ_0.

It has been shown in the literature [5, 6, 10, 12] that a simple single-polar-phonon-mode model with a frequency-independent damping constant Γ_0 cannot describe correctly the dispersion relation and damping of the polaritons in $LiNbO_3$ and $LiTaO_3$. To account for additional modes in the spectra, which are not extended phonon modes of A_1 symmetry, low-frequency modes have been introduced. In $LiNbO_3$ some of these modes were traced back to a coupling to E phonon modes and defect modes [6, 10, 12]. The low-frequency modes can be included in the model in two different ways: first, by coupling low-frequency excitations to the mechanical part of the polariton [5, 10, 20, 21] (M coupling) and, second, by assuming that these excitations have oscillator strengths providing a coupling to the electric field [19] (E coupling).

In the M-coupling model the damping of the polariton is increased by coupling low-frequency modes $(1 \ldots N)$ to the polariton, representing an energy flow from the polariton to

the low-frequency modes. It can be described by replacing Γ_0 in equation (1) or (7) by an effective damping function

$$\Gamma_{\text{eff}}(\omega) = \Gamma_0 + \frac{1}{\mathrm{i}\omega}\left[\sum_{j=1}^{N} \frac{K_j}{\omega_j^2 - \omega^2 - \mathrm{i}\omega\Gamma_j} + \frac{\delta^2}{1 - \mathrm{i}\omega\tau}\right]. \tag{8}$$

The sum in the square brackets takes into account the coupling of the mechanical part of the polariton to N low-frequency excitations of frequency ω_j, damping constant Γ_j and coupling constant K_j. To account for an inhomogeneous broadening of a low-frequency mode, the corresponding term in equation (8) is replaced by a Voigt profile of inhomogeneous linewidth $\delta\omega_j$ similar to the second term on the right-hand side of equation (7).

In the E-coupling model a dielectric function $\varepsilon(\omega)$ similar to that in the M model can be generated with a different set of parameters for the low-frequency modes. All forward scattering Raman experiments are determined in a good approximation only by the dielectric function and thus cannot distinguish between the two coupling schemes. In 90° and backward scattering Raman experiments the E model provides the nonlinear coefficients d'_{Q_j} for each low-frequency mode as an additional parameter. So even the combination of all performed experiments does not allow us to distinguish between the two models. For this reason we treat the experimental data in the M model, only. A mixture of both coupling schemes could be possible, too.

Figure 1 shows an example of the influence of the M coupling of one low-frequency mode (at about 90 cm^{-1}) to the polariton on the Raman gain factor. Due to the increase of the damping of the polariton in this frequency region the Raman linewidth is broader (not seen in figure 1) and the peak gain factor is reduced, which is clearly visible as a minimum in figure 1. At the same time a ridge stretches out parallel to the $\boldsymbol{k}$ axis, causing a small peak of the spontaneous Raman spectrum at the frequency of the low-frequency mode (90 cm^{-1}).

$LiTaO_3$ is a ferroelectric crystal, for which it has been shown that a Debye relaxational mode strongly influences the spontaneous Raman spectrum [23–26]. We take this mode into account by the second term in the square bracket in equation (8). The Debye relaxational mode has a coupling strength δ^2 and a relaxation time τ.

3. Experimental results and discussion

The experimental methods used in this paper will be presented only briefly, because they have been described in detail elsewhere [6, 10, 12, 27]. All experiments were carried out in an individual congruent $LiTaO_3$ single crystal ($20 \times 8 \times 10$ mm^3) at liquid nitrogen (77 K) and room temperature (295 K). The laser beams were polarized parallel to the optical c axis of the crystal to excite polaritons of A_1 symmetry. All wavevectors were in the isotropic x–y plane of the crystal.

3.1. Spontaneous Raman scattering

Spontaneous Raman spectra at a scattering angle of 90° were measured using an Ar^+ laser at 488 nm, a double monochromator with a spectral resolution of 1 cm^{-1} and a photon counting system [27]. This scattering angle corresponds to a large polariton wavevector, i.e., in fact information on the corresponding phonon is obtained.

The spectra for a Raman shift up to 300 cm^{-1} are shown in figure 2 as shaded areas for $T = 77$ and 295 K. They are dominated by the lowest A_1 phonon mode, which has a strongly asymmetric line shape with the maximum at 211 and 203 cm^{-1} at 77 and 295 K, respectively. In order to show more clearly the weak Raman lines the Raman intensity has been multiplied

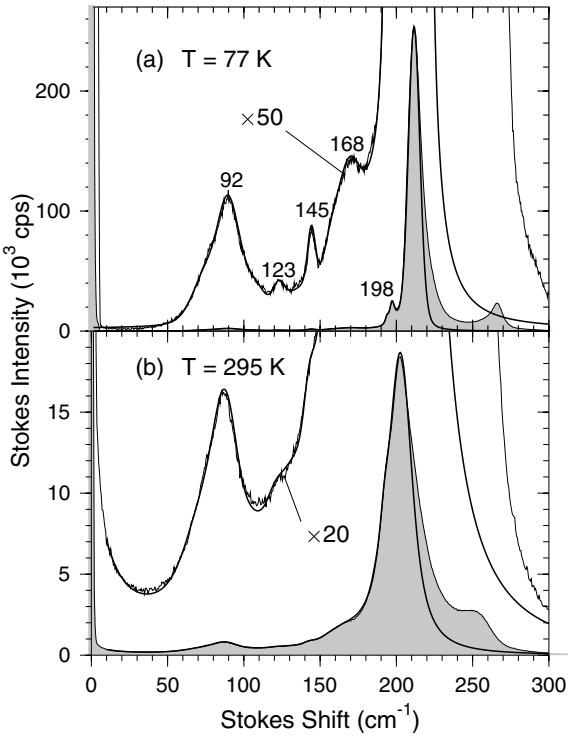

Figure 2. Spontaneous 90° Raman spectrum of congruent $LiTaO_3$ (shaded area and thin solid curves) in the A_1 mode geometry at (a) 77 K and (b) 295 K. Upper curves: magnified spectrum. Thick curve: spontaneous Raman spectrum calculated from equations (6)–(8). Low-frequency modes and for room temperature the Debye relaxation were taken into account.

by factors of 50 and 20 at 77 and 295 K, respectively. The noisy curves represent the measured spectrum; the solid curves have been calculated (see below).

Since the low-frequency wing of the A_1 mode has a Gaussian shape at $T = 77$ K, we assumed that it is inhomogeneously broadened, i.e., we used the integral in equation (7) in the calculations. At $T = 77$ and 295 K the inhomogeneous linewidth $\delta\omega_0$ and homogeneous linewidth Γ_0 is predominant, respectively. We did not attempt to get a fit for the high-frequency side of the measured line.

On the low-frequency wing of the strong A_1 Raman line, weak lines at 92, 123, 145, 168 and 198 cm^{-1} are clearly visible at 77 K (figure 2(a)). There has been a detailed discussion of the weak low-frequency Raman lines and absorption bands by Wiederrecht *et al* [5]. The lines at 145 and 198 cm^{-1} have been ascribed to E modes [23, 28, 29] of $LiTaO_3$ which couple to the A_1 mode because of the presence of strain in the crystal [30]. The line at 92 cm^{-1} has been ascribed to a two-phonon difference band [23, 24]. But we dispute the latter interpretation because the temperature dependence of the band intensity, which we measured from 30 to 295 K does not agree with that expected for a two-phonon difference band. We tentatively ascribe this weak line to a defect mode in $LiTaO_3$ in analogy to $LiNbO_3$ [6]. The other weak lines at 123 and 168 cm^{-1} are low-frequency excitations of unknown nature.

The weak lines on the low-frequency wing of the 203 cm^{-1} A_1 mode are caused by the low-frequency excitations. A detailed analysis of the structure of the low-frequency wing shows that in addition to the low-frequency excitations discussed above further weak excitations have

Table 1. Fit parameters determined at $T = 77$ K for the coupling of low-frequency excitations to the mechanical part of the polariton. The eigenfrequency $\bar{\nu}_j$, homogeneous linewidth Γ_j, inhomogeneous linewidth $\delta\bar{\nu}_j$ and coupling coefficient $K_j^{(sp)}$ of mode j have been determined from the 90° spontaneous Raman data. The coupling coefficient $K_j^{(stim)}$ was obtained from gain measurements of SRS. At $T = 77$ K no contribution of the Debye relaxational mode was observed. The error margin for the K_j is ±20%. Numbers for the main A_1 mode: eigenfrequency $\bar{\nu}_0 = 209.2$ cm^{-1}, oscillator strength $S_0 = 25.2$, homogeneous and inhomogeneous linewidth $\Gamma_0 = 1.1$ and $\delta\bar{\nu} = 5.2$ cm^{-1}, nonlinear coefficient $d'_Q = 9.8$ pm V^{-1}.

$\bar{\nu}_j$ (cm^{-1})	Γ_j (cm^{-1})	$\delta\bar{\nu}_j$ (cm^{-1})	$K_j^{(sp)}$ (10^6 cm^{-4})	$K_j^{(stim)}$ (10^6 cm^{-4})
77	6	11	2.4	1.4
92	4.5	9	6.2	3.6
108	7	7	1.7	1.4
123	3	5	0.9	0.6
135	6	9	1.2	1.0
145	2.5	3	1.1	0.6
156	4	7	1.2	1.4
168	7	9	3.7	2.2
184	5	9	0.6	0.1
194	2.5	0	0.25	0.05
198	4.2	0	1.35	0.5

to be included. It is important to note that most of the weak Raman lines have steeply decreasing wings. This and the low Raman signal in the frequency range below 60 cm^{-1} at $T = 77$ K can be explained only if these low-frequency modes are inhomogeneously broadened. Considering the inhomogeneous broadening of the main line and the defect mode nature of part of the low-frequency modes, this is a reasonable assumption. For the inhomogeneously broadened lines the resonance denominators in equations (8) have been replaced by integrals similar to the second term in equation (7).

The numbers obtained from the fits are collected in table 1 for $T = 77$ K and table 2 for $T = 295$ K. The numerous overlapping low-frequency modes do not allow an accurate determination of the homogeneous and inhomogeneous contributions to the line broadening, so numbers for Γ_j and $\delta\bar{\nu}_j = \delta\omega_j/(2\pi c)$ in tables 1 and 2 have to be considered with caution. In addition, at 295 K a Debye relaxational mode was included to describe the broad wing close to the laser line correctly (figure 2(b)).

3.2. Stimulated Raman gain factor

In the SRS amplifier experiment [6, 10] a pump laser beam of frequency ω_L (frequency-doubled Q-switched Nd:YAG laser) and a tunable dye laser beam at the Stokes frequency ω_S excite a polariton with frequency $\omega = \omega_L - \omega_S$ and wavevector $\boldsymbol{k} = \boldsymbol{k}_L - \boldsymbol{k}_S$. The stimulated Raman gain is measured in the near forward direction with a small angle $\vartheta \approx 0.2 \ldots 15°$ between laser and Stokes beam. From the measured amplification of the Stokes beam the gain factor $g_S(\omega, k)$ is calculated, taking into account the spatial overlap of pump and Stokes beam [6].

Gain curves for stimulated scattering from polaritons were measured in congruent $LiTaO_3$ in the A_1 mode geometry in two ways:

(i) by varying the Stokes frequency at constant angle ϑ between pump and Stokes beam, i.e., nearly constant polariton wavevector (see figure 1, dotted curve),

Table 2. Fit parameters determined for $T = 295$ K. Debye relaxational mode: $\tau = 0.6$ ps, $\delta^2 = 700$ cm^{-2}. The error margin for the K_j is ±50%. Main A_1 mode: $\bar{\nu}_0 = 198$ cm^{-1}, $S_0 = 29.8$, $\Gamma_0 = 14$ cm^{-1}, $\delta\bar{\nu} = 5.2$ cm^{-1}, $d'_Q = 9.8$ pm V^{-1}. At room temperature spontaneous and stimulated Raman experiments can be described with one parameter set, so only one value for K_j is listed.

$\bar{\nu}_j$ (cm^{-1})	Γ_j (cm^{-1})	$\delta\bar{\nu}_j$ (cm^{-1})	K_j (10^6 cm^{-4})
74	16	11	2.5
89	8	9	5.4
106	12	7	1.8
121	14	5	1.8
132	14	9	1.4
143	8	3	1.2
155	8	7	2
166	8	9	4.5
180	9	9	0.8
186	8	0	0.3
192	8	0	1.2

(ii) by varying the angle ϑ and keeping the Stokes frequency constant (see figure 1, dashed curve).

We determined the heights g_S and widths $\delta\bar{\nu}_G$ and δk_G of the gain curves (methods (i) and (ii), respectively). The peak gain factor g_S has a lower measurement accuracy, due to its dependence on the overlap of Stokes and pump beam, and is therefore not discussed.

The measured widths $\delta\bar{\nu}_G$ and δk_G of the gain curves are plotted in figure 3 and on the right-hand side of figure 4, respectively, as closed ($T = 77$ K) and open ($T = 295$K) circles together with the calculated curves versus polariton frequency $\bar{\nu}$. The low-frequency excitations, which were observed in the spontaneous Raman spectra, have a strong influence on the Raman linewidth. At the resonance frequencies $\bar{\nu}_j$ (dotted vertical lines in figures 3 and 4) of these excitations the damping of the polariton is high, leading to maxima of the Raman linewidth $\delta\bar{\nu}_G$ and absorption coefficient $\alpha \approx \delta k_G$.

Below $\bar{\nu} \approx 70$ cm^{-1} the polariton damping is so low that polaritons are travelling macroscopic distances and are leaving the interaction region of the pump and Stokes laser beam in the Raman amplifier experiment. This acts as an additional damping effect [6] and causes the approximately constant linewidth $\delta\bar{\nu}_G$ in the limit of low polariton frequencies in figure 3.

A comparison between the Raman linewidths $\delta\bar{\nu}_G$ at different temperatures shows that the polariton damping at room temperature is higher by about a factor of two to four compared to $T = 77$ K (note different vertical scales in figures 3(a) and (b)). This is due to the fact that the coupling constants K_j of the low-frequency excitations are larger at room temperature. In addition, the width of the 203 cm^{-1} A_1 mode line is broader at room temperature, providing a higher damping background at all polariton frequencies (see figure 3(b)).

To compare the experimental results with calculations we have analysed the Raman gain factor using the approximation $g_S \propto \mathrm{Im}\{(c^2k^2/\omega^2 - \varepsilon)^{-1}\}$ (see section 2.1) and including all extensions in the M-coupling scheme. In this way the dielectric function $\varepsilon(\omega)$ and coupling constants K_j of the modes are determined from the frequency dependence of the Raman linewidth $\delta\bar{\nu}_G$ obtained in the stimulated Raman gain measurements. The numbers for the frequencies ω_j and damping constant Γ_j of the low-frequency excitations were taken from the spontaneous Raman measurements.

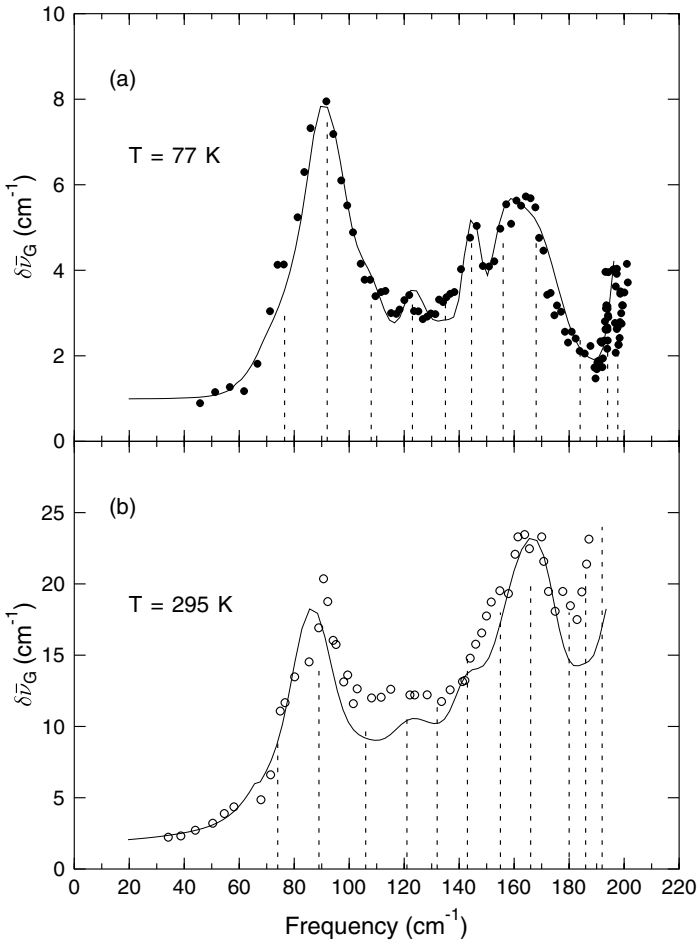

Figure 3. Line widths $\delta\bar{\nu}_G$ of the Raman gain curves as a function of polariton frequency. The filled circles show the experimental data at (a) 77 K and the open circles at (b) 295 K. The solid curve represents the calculations. The dotted vertical lines mark the positions of the eigenfrequencies of the low-frequency modes.

Measured values of the width δk_G are shown in figure 4 (right-hand side) together with curves of the absorption coefficient $\alpha(\bar{\nu})$ for both temperatures, using the same parameters as for $\delta\bar{\nu}_G$ in figure 3. The good agreement of experimental and theoretical values in figures 3 and 4 (right-hand side) for the same model parameters confirms the identification of δk_G with the spatial damping α.

We have also determined the dispersion curve of the polaritons from the positions of the maxima of the measured gain curves. The experimental results for 77 K are shown in figure 5 as solid points. The solid line has been calculated without low-frequency modes by using equation (1). It is interesting to note that the coupling of the 197.7 cm^{-1} mode to the polariton is so strong that there is an avoided crossing of the dispersion curve.

The accuracy of the measured dispersion curve is so high that we chose a different way of presentation to visualize the influence of the low-frequency modes on the polariton dispersion. In figure 6 the frequency difference $\Delta\bar{\nu}$ between the measured dispersion curve

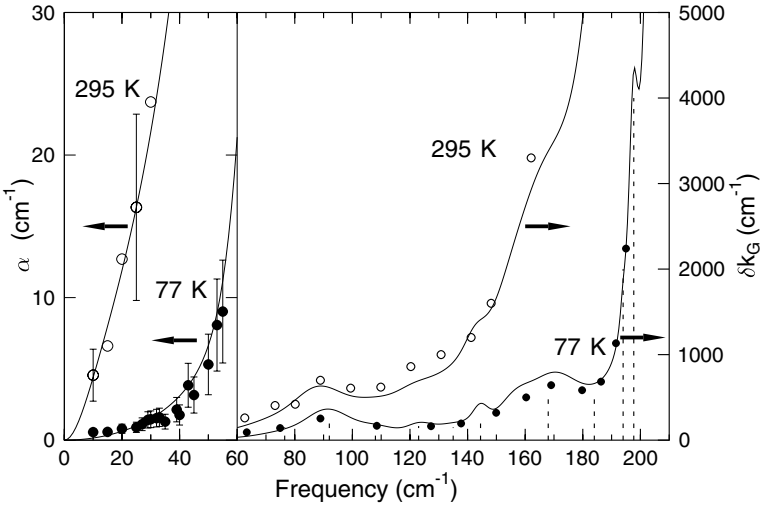

Figure 4. Polariton absorption coefficient versus polariton frequency $\bar{\nu}$ at 77 and 295 K (filled and open circles, respectively). The solid curve has been calculated. Left-hand side: polariton absorption coefficient α measured with the nonlocal time-delayed CARS method. Right-hand side: width δk_G of the Raman gain curve. Note the different ordinate scales on the left- and right-hand sides.

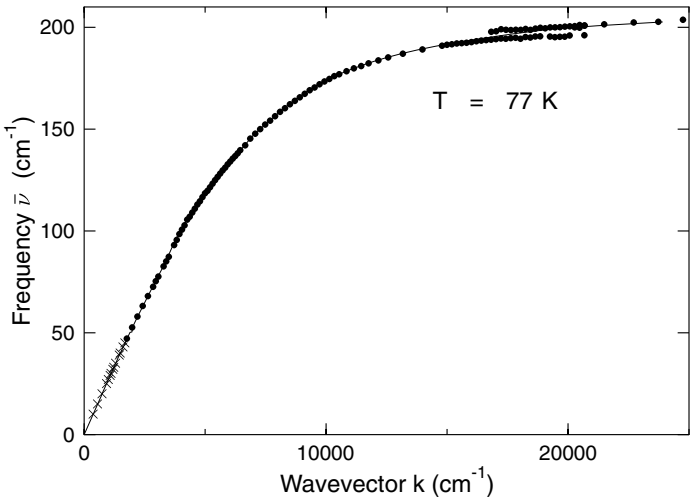

Figure 5. Polariton dispersion curve. The solid points and crosses have been measured at 77 K using the Raman gain and the nonlocal time-delayed CARS method, respectively. The solid curve has been calculated without low-frequency modes.

and the calculated one *without* low-frequency modes is plotted versus polariton frequency $\bar{\nu}$ (solid points). The solid curve represents the difference between the calculated dispersion relation with and without low-frequency excitations. Close to the resonance frequencies $\bar{\nu}_j$ (dotted vertical lines) of the low-frequency modes both measurement and calculation show the same bending of the dispersion curve. In particular, the large variations caused by the avoided crossing at 197.7 cm^{-1} are clearly visible. For all other low-frequency modes the coupling coefficient is too low or the damping is too high to cause an avoided crossing.

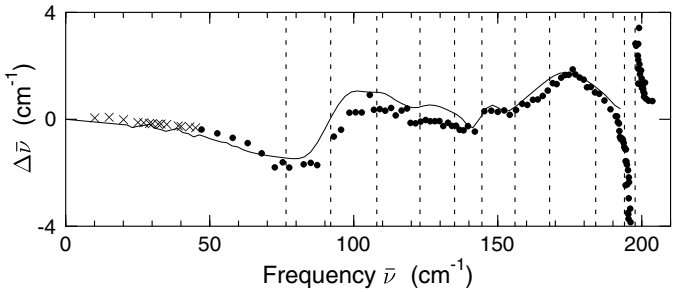

Figure 6. Frequency difference $\Delta\bar{\nu}$ between the measured polariton dispersion curve and the calculated one without low-frequency modes. The solid points and crosses have been measured at 77 K using the Raman gain and the nonlocal time-delayed CARS method, respectively. The solid curve corresponds to the frequency difference of the calculated dispersion with and without low-frequency modes. The dashed vertical lines show the resonance frequencies.

We conclude that the observed effects of the low-frequency modes on the damping of the polaritons and on the dispersion curve are described very well by our model calculations. It is emphasized that one set of parameters is used to calculate the linewidth $\delta\bar{\nu}_G$ in figure 3, spatial damping α in figure 4 and polariton dispersion curve in figure 5.

We have compared our experimental results for the Raman linewidth $\delta\bar{\nu}_G$ at room temperature (figure 3(b)) with that of Wiederrecht *et al* [5] who used impulsive SRS with femtosecond laser pulses. There is good agreement between both methods for polariton frequencies between 30 and 160 cm^{-1}. Above 160 cm^{-1} there is just one single experimental point in [5] to compare with.

3.3. Time-delayed CARS technique

With nonlocal time-delayed CARS we have measured the absorption coefficient α and the group velocity v_{gr} of freely propagating polaritons in congruent $LiTaO_3$. Polariton pulses were excited by a mode-locked Nd:YAG laser (wavelength 1.064 μm, pulse duration 35 ps) and a tunable optical parametric oscillator which provide the pump and Stokes frequency, respectively [12]. The polariton pulses were detected after propagating freely a certain distance in the isotropic plane of the crystal by time-delayed, properly phase-matched CARS of a probe pulse (second harmonic of the pump pulse). By measuring the CARS energy for a definite delay time between the probe and pump pulses at different positions in the crystal a snapshot of the polariton pulse was obtained. From snapshots at different delay times the propagation velocity and the absorption coefficient α of the polaritons are determined.

The experimental points for the absorption coefficient α of $LiTaO_3$ are shown for 77 and 295 K (full and open circles) on the left-hand side of figure 4 together with the calculated curves. The calculated curves are the continuation of the curves on the right-hand side of the figure with an extended scale of the ordinate. There is good agreement between the experimental points and the calculated curves, indicating that the results of both the propagation experiment and the gain measurement can be described with our model with the same set of parameters.

At room temperature (open circles in figure 4) the absorption coefficient α is so high that measurements were possible only up to 30 cm^{-1}. At this frequency (0.95 THz) a low-frequency excitation has been found in [19], which was not observed in our measurements and might be weak or absent in our crystal. The absorption coefficient α at room temperature is essentially determined by the coupling of the polaritons to the low-frequency excitations

at 76 and 92 cm^{-1} and to the Debye relaxational mode, which has also been observed in the spontaneous Raman spectrum (see broad wing close to the laser line in figure 2(b)). In addition, the wing of the A_1 phonon mode at 203 cm^{-1} provides a significant contribution to the absorption of the polaritons even at this low frequency.

At $T = 77$ K the absorption coefficient α could be measured by CARS up to 55 cm^{-1} (solid circles in figure 4). Polariton damping in this frequency region at low temperatures is caused by the lowest two low-frequency modes and by the low-frequency wing of the A_1 phonon. The results from the CARS and SRS experiment can be described by one set of parameters (table 1 and calculated solid curve in figure 4). The combination of both experiments provides the damping of polaritons in $LiTaO_3$ at 77 K in a continuous frequency band from 10 to 195 cm^{-1}.

From the measured dependence of the group velocity on the polariton frequency the dispersion curve $\bar{\nu}(k)$ was calculated up to about 60 cm^{-1} using the definition of $v_{gr} = 2\pi c\, d\bar{\nu}/dk \approx 2\pi c(\bar{\nu}_n - \bar{\nu}_{n-1})/(k_n - k_{n-1})$. Here, $\bar{\nu}_n$ $(n = 1, 2, \ldots)$ is the polariton frequency at which the group velocity v_{gr} was measured. Using the measured values for $\bar{\nu}_n$ and v_{gr}, we calculated the wavevectors k_n step by step and obtained the dispersion relation (crosses in figures 5 and 6). It should be noted that the accuracy of these measurements (about $\pm 10\%$) is lower than that of the SRS gain measurements (about $\pm 2\%$). There is again good agreement with the calculated curves.

3.4. Discussion

At room temperature all three Raman experiments (spontaneous 90° Raman scattering, forward SRS and polariton propagation) can be described within the context of the linear response theory for phonon-polariton Raman scattering. Only one parameter set for the low-frequency modes is needed to describe all experimental data sets (see table 2). But one has to be aware that many of the low-frequency excitations are not very pronounced at room temperature. Differences observed at low temperature might easily be masked at room temperature by measurement uncertainties.

At $T = 77$ K the forward SRS gain experiment (polariton frequencies $\bar{\nu} > 70$ cm^{-1}) and the polariton propagation experiment ($\bar{\nu} < 70$ cm^{-1}) can be described with one set of parameters. The gain widths $\delta\bar{\nu}_G$ and δk_G measured in the forward SRS experiment depend to a good approximation only on the frequency-dependent damping of the phonon polariton and thus on the complex dielectric function ε (see section 2.2). The absorption coefficient α measured in the propagation experiment is also derived from this dielectric function.

The spontaneous 90° Raman measurement at $T = 77$ K cannot be described with the same parameter set as the forward SRS gain measurement. Different coupling constants $K_j^{(sp)}$ and $K_j^{(stim)}$ have been obtained by fitting the spontaneous and stimulated Raman measurements using equations (6) and (3), respectively. A closer look at tables 1 and 2 shows that the coupling constants $K_j^{(sp)}$ do not change very much in going from room temperature to 77 K, at least for the stronger low-frequency modes. In contrast, the coupling constants $K_j^{(stim)}$ are lower by approximately a factor of 2 when the temperature is decreased.

Because spontaneous Raman scattering was performed at 90° and the SRS gain measurement in the near forward direction, a dependence of the coupling constants on the polariton wavevector is a possible interpretation for the difference between $K_j^{(sp)}$ and $K_j^{(stim)}$. As a consequence the dielectric function would depend both on frequency and wavevector of the phonon polariton and would have to be written as $\varepsilon(\bar{\nu}, k)$. This behaviour is even likely if the low-frequency mode is a localized excitation associated with a crystal defect and couples to the extended A_1 phonon polariton. However the problem is that this effect should be observed both at low temperature and at room temperature.

At 77 K there are experimental problems which may influence the measurements. The photorefractive effect [2] is more effective at low temperatures and can change the laser beams depending on their intensity. In addition strain-induced birefringence in the crystal may change the polarization of the light beams. Both effects can be different for the spontaneous and stimulated Raman measurements and may cause the observed differences.

Another problem is that the nature of most of the low-frequency excitations is not known. We have assumed that their behaviour and coupling to the polaritons can be described by a simple damped harmonic oscillator equation. This may not be correct e.g. if the low-frequency excitations are flat electronic traps. The population of such traps normally depends on temperature, an effect which has not been taken into account in our calculations.

Our low-temperature experiments are in contradiction to the interpretation of the low-frequency modes as transitions between higher levels in an asymmetric double-well potential, given by Bakker *et al* [19, 21]. First these levels are unoccupied at $T = 77$ K and associated low-frequency modes should not be observed at this temperature. Second the different frequencies and strengths of the low-frequency modes as observed by different groups suggest their dependence on doping and stoichiometry of the individual crystal, similar to observations made in $LiNbO_3$ [6]. For the levels in an asymmetric double-well potential connected with the ferroelectric phase transition this behaviour would not be expected. Impulsive Raman scattering experiments by Bakker *et al* did show pronounced avoided crossings of the dispersion curve at 32 cm^{-1} [9, 19] and 44, 80, 115 and 138 cm^{-1} [21]. In contrast to this a recent reinvestigation of the A_1 phonon polariton by impulsive SRS did not show a splitting of the dispersion curve in the frequency range from 15 to 140 cm^{-1} [31, 32]. This is in accordance with our measurements (see figures 5 and 6) and leaves the mode at 198 cm^{-1} as the only low-frequency mode causing an avoided crossing of the dispersion curve.

4. Conclusions

We have investigated the damping and dispersion of phonon polaritons of the lowest A_1 mode of $LiTaO_3$ in the frequency range from 10 to 200 cm^{-1} using different methods of Raman spectroscopy. For polaritons below 70 cm^{-1}, where damping is low and the polariton propagates over a macroscopic distance, the nonlocal time-delayed CARS method is the method of choice. It allows a direct and precise measurement of the polariton damping and group velocity. Impulsive Raman scattering has an upper frequency limit, determined by the finite duration of the femtosecond pump and probe pulses, which have to be short compared to one polariton cycle. The SRS gain experiment on the other hand can address the whole polariton branch up to frequencies close to the optical phonon mode (about 200 cm^{-1} in $LiTaO_3$) with high spectral resolution, but is limited at low frequencies (<70 cm^{-1}) by an artificial damping introduced by the macroscopic propagation of the polariton. These methods are used in the near forward direction and probe the polariton dispersion for small wavevectors. For large wavevectors, where the dispersion is negligible, spontaneous Raman scattering provides most information on resonance frequency, linewidth and shape of extended phonon modes and low-frequency excitations. Together these Raman experiments cover the whole two-dimensional ω–k range of the phonon-polariton dispersion, but the overlap of the methods, dictated by polariton propagation and spatial dispersion, is small.

An analysis of our experimental data showed that the damping of phonon polaritons with frequencies between 10 and 70 cm^{-1} at 77 K is essentially determined by the low-frequency wing of the A_1 phonon mode and contributions from the low-frequency excitations at 76 and 92 cm^{-1}. The strong increase of the damping from 77 K to room temperature is caused by the broader linewidth of the A_1 phonon mode and the increase of the coupling constants of the

low-frequency excitations. In addition there is a Debye relaxational mode, which contributes to the damping of the phonon polaritons at low frequencies.

In the frequency range from 70 to 200 cm^{-1} the observed peaks in the phonon-polariton damping have been attributed to the coupling of the polaritons to low-frequency excitations. The reason for the increase of the damping from 77 K to room temperature is the same as in the lower-frequency range, namely the increase of the linewidth of the A_1 phonon mode and of the coupling constants of the low-frequency excitations. We have determined all relevant parameters of the low-frequency excitations at 77 K and room temperature: the resonance frequencies, homogeneous and inhomogeneous line widths, non-linear coefficients, coupling constants to the mechanical part of the polariton and the relaxation time and coupling constant of the Debye relaxational mode.

In addition we have determined the dispersion relation of the phonon polaritons between 10 and 200 cm^{-1} with high accuracy. It shows a very subtle fine structure which is caused by the coupling of the low-frequency excitations to the phonon polaritons.

We used a linear response theory to describe spontaneous 90° Raman scattering and the near forward SRS gain experiment within one formalism. The underlying complex dielectric function determines also the damping of freely propagating polaritons detected by nonlocal time-delayed CARS or in the impulsive Raman experiment. At room temperature all Raman data could be described with one set of material parameters.

At low temperatures ($T = 77$ K) only the experimental results for forward SRS and phonon propagation detected by nonlocal time-delayed CARS could be described with one set of parameters for the dielectric function. In the comparison of spontaneous 90° Raman scattering and forward SRS it was found that different coupling constants of the low-frequency excitations to the polaritons were needed to describe the experimental results with the linear response theory. We discussed several possible causes for the discrepancies between theory and experiments, including a possible dependence of the dielectric function on the wavevector of the polariton, and the nature and theoretical treatment of the widely unknown low-frequency excitations.

References

[1] Hikita T 2001 *Ferroelectrics and Related Substances* ed Y Shiozaki, E Nakamura and T Mitsui (Berlin: Springer) p 548
[2] Krätzig E and Schirmer O F 1988 *Photorefractive Materials and Their Applications* ed P Günter and J-P Huignard (Berlin: Springer) p 131
[3] Bakker H J, Hunsche S and Kurz H 1998 *Rev. Mod. Phys.* **70** 523
[4] Auston D H and Nuss M C 1988 *IEEE J. Quantum Electron.* **24** 184
[5] Wiederrecht G P, Dougherty T P, Dhar L, Nelson K A, Leaird D E and Weiner A M 1995 *Phys. Rev.* B **51** 916
[6] Schwarz U T and Maier M 1998 *Phys. Rev.* B **58** 766
[7] Schirmer O F, Reyker H-J and Wöhleke M 1995 *Insulating Materials for Optoelectronics* ed T Aquilló-López (Singapore: World Scientific)
[8] Wiederrecht G P, Dougherty T P, Dhar L, Nelson K A, Leaird D E and Weiner A M 1993 *Ferroelectrics* **150** 103
[9] Bakker H J, Hunsche S and Kurz H 1992 *Phys. Rev. Lett.* **69** 2823
[10] Schwarz U T and Maier M 1996 *Phys. Rev.* B **53** 5074
[11] Vallée F and Flytzanis C 1992 *Phys. Rev.* B **46** 13 799
[12] Qiu T and Maier M 1997 *Phys. Rev.* B **56** R5717
[13] Dougherty T P, Wiederrecht G P and Nelson K A 1992 *J. Opt. Soc. Am.* B **9** 2179
[14] Koehl R M, Adachi S and Nelson K A 1999 *J. Chem. Phys.* **110** 1317
[15] Adachi S, Koehl R M and Nelson K A 2000 *J. Lumin.* **87–89** 840
[16] Barker A S Jr and Loudon R 1972 *Rev. Mod. Phys.* **44** 18
[17] Henry C H and Garrett C G B 1968 *Phys. Rev.* **171** 1058

[18] Sussman S S 1970 *ML Report* No 1851 *(Stanford)*
[19] Bakker H J, Hunsche S and Kurz H 1993 *Phys. Rev.* B **48** 9331
[20] Barker A S Jr 1968 *Phys. Rev.* **165** 917
[21] Bakker H J, Hunsche S and Kurz H 1994 *Phys. Rev.* B **50** 914
[22] Yariv A 1988 *Quantum Electronics* (New York: Wiley) p 407
[23] Raptis C 1988 *Phys. Rev.* B **38** 10 007
[24] Tezuka Y, Shin S and Ishigame M 1994 *Phys. Rev.* B **49** 9312
[25] Penna A F, Chaves A and Porto S P S 1976 *Solid State Commun.* **19** 491
[26] Zhang M and Scott J F 1986 *Phys. Rev.* B **34** 1880
[27] Schwarz U T and Maier M 1997 *Phys. Rev.* B **55** 11 041
[28] Yang X, Lan G, Li B and Wang H 1987 *Phys. Status Solidi* **141** 287
[29] Barker A S Jr, Ballmann A A and Ditzenberger J A 1970 *Phys. Rev.* B **2** 4233
[30] Johnston W D Jr and Kaminov I P 1968 *Phys. Rev.* **168** 1045
[31] Watanuki T, Yoshioka S, Kasahara M, Crimmins T F, Nelson K A and Yagi T 2001 *J. Phys. Soc. Japan* **70** 2784
[32] Crimmins T F, Stoyanov N S and Nelson K A 2002 *J. Chem. Phys.* **117** 2882